Spray drying as a viable process to produce nano-hydroxyapatite/chitosan (n-HAp/CS) hybrid microparticles mimicking bone composition

G. Ruphuy [a,b], A. Saralegi [b], J.C. Lopes [a], M.M. Dias [a], M.F. Barreiro [b]

[a] *Laboratory of Separation and Reaction Engineering (LSRE) – Associate Laboratory LSRE-LCM, Faculty of Engineering, University of Porto, Porto, Portugal*

[b] *Laboratory of Separation and Reaction Engineering (LSRE) – Associate Laboratory LSRE-LCM, Bragança Polytechnic Institute, Bragança, Portugal*

Abstract

In this work nano-hydroxyapatite/chitosan (n-HAp/CS) hybrid microparticles were prepared by spray drying following a methodology where, in a first step, aqueous nanodispersions of n-HAp in the presence of chitosan were produced by fast stirring at pH values below and above chitosan pKa (5.5 and 7.0, respectively). The mixing system used allowed the production of homogeneous and stable nanodispersions, and the subsequent spray-dried microparticles, incorporating highly pure HAp nanoparticles of approximately 50 nm, were successfully produced without degrading the organic component, chitosan. Comparatively with the n-HAp/CS-7.0, the n-HAp/CS-5.5 dispersions were characterized by a lower particle size and a higher zeta potential, being then more stable. Differences in the spray-dried microparticles were also evident from a morphological point of view. HApCS-5.5 microparticles, which present an average size in volume of 15.8 μm and n-HAp crystals homogenously distributed, were found to be preferred over the HApCS-7.0 counterparts, which require an extra step in the productive process and presented a tendency to form large agglomerates. Both prepared hybrid particles presented similar composition to that one of natural bone (HAp/CS of 70/30) and no traces of KCl salts were observed if a washed n-HAp paste was used.

Keywords: Bone tissue analogues; Microparticles; Nano-hydroxyapatite; Chitosan; Spray-drying

1. Introduction

Natural bone is a complex and highly organised nanocomposite composed of approximately 60–70% hydroxyapatite ($Ca_{10}(PO_4)_6(OH)_2$, HAp) nanocrystals precipitated onto 25–30% of collagen fibers, and a small portion of water [1,2]. With the aim of emulating natural bone, efforts have been focused in combining biodegradable polymers with ceramic materials, particularly calcium phosphates (Ca-P), to mimic the organic and inorganic components of bone. In this context, a common suitable hybrid system for bone tissue engineering consists in the combination of hydroxyapatite (HAp) with chitosan (CS) [3].

Chitosan (CS), the main derivative of natural polymer chitin, presents a wide list of desirable properties for bone repair and regeneration, namely: biocompatibility [4,5]; mucoadhesiveness [6,7]; hydrophilic character which promotes osteoblast adhesion and proliferation [8]; wound healing properties [9,10]; and non-toxicity of its biodegradation products [11,12]. Most of these properties are due to chitosan's structure; this polymer contains in its main backbone primary amine groups that become positively charged in acidic medium. This cationic character of chitosan is what makes it both reactive and soluble depending on the pH. With a pKa value around 6.5, chitosan is insoluble in neutral and alkaline pH solutions, but it is soluble in aqueous acidic medium, allowing it to be processed under mild conditions [2,12]. In addition, chitosan can be shaped into different forms such as porous scaffolds [13–15], fibers [16,17], sponges [8] and microparticles [18–20], an advantageous feature for tissue engineering applications [21].

Hydroxyapatite, on the other hand, is a double salt of tricalcium phosphate and calcium hydroxide ($Ca_{10}(PO_4)_6(OH)_2$). With a Ca/P ratio of 1.67, it is the most stable and less soluble Ca–P ceramic under physiological conditions (pH ~ 7). However, below a pH of 4.8, HAp becomes gradually soluble and the formation of monetite ($CaHPO_4$) is favoured [22]. In its nanometric form, nanohydroxyatatite (n-HAp) is more advantageous to the conventional micrometric sized HAp in what concerns the promotion of osteoblast. adhesion, differentiation and proliferation, osteointegration, and deposition of Ca-containing minerals on its surface [23,24].

The combination of HAp with chitosan for bone tissue engineering applications is typically based in the production of porous scaffolds [25–27]; nonetheless, advances in science and technology have led to the development of particulate materials that, thanks to their reduced size, can be suitable as injectable systems or shaped into a solid substrate with increased surface area that will promote chemical and biological reactions [28–30]. In this context, the development of a particulate system containing n-HAp in a micrometer-sized matrix is advantageous; this approach allows HAp's superior properties at the nanoscale to be preserved in the form of microparticles that are easier to handle [31].

Among the existing techniques, spray drying appears as a promising technology manufacturing microparticles with controllable size and morphology [32]. It is a process widely used as a microencapsulation/stabilization technique in the food [33,34] and pharmaceutical [35,36] industries. Easy industrialization, cost-effectiveness and continuous production are attractive features of this technique; however prolonged contact with high temperatures can cause product degradation [37]. This method is based in the drying of atomized droplets of a previously prepared dispersion using a co-current stream of hot gas, and the preparation of this dispersion is also a key step in the overall process.

One of the most common established methods used to prepare HAp/CS hybrid dispersions consists in mixing previously prepared HAp microparticles, usually as a powder, into a chitosan solution. This technique can lead to non-homogenous dispersions at a microscopic level, due to the difficulty in controlling the mixing between two dissimilar phases that can lead to phase separation. In efforts to overcome such problem, an adequate incorporation of HAp into the chitosan matrix has been reported [23,38] by using the so-called co-precipitation method; nevertheless, this method implies the synthesis of HAp in the presence of chitosan, which hinders the formation of HAp particles with high purity and desired morphology.

Another important parameter to consider when preparing n-HAp/CS hybrid dispersions is pH, especially if HAp has to be introduced into an acidic environment that can influence its solubility, chemistry and phase stability [39]. In the simple mixing method, HAp is often introduced in an acidic chitosan solution, resulting in dispersions with pH typically around 4–5. In the case of the co-precipitation method, the combination of both components is carried out in a neutral or basic environment ($pH \geq 7$), causing the precipitation of chitosan along with HAp simultaneously.

Basargan et al. (2015) [40] appears to be the only one work reporting the production of HAp/CS microparticles by spray drying. Here a HAp/CS-slurry using co-precipitation method ($pH \geq 9.0$) was prepared, followed by spray drying. The effect of inlet temperatures (120 °C and 160 °C) and different HAp/CS weight ratios was studied. Spherical microparticles of mean size 4–6 μm were produced, and an increase in surface area with the addition of chitosan, as well as with the highest inlet temperature, were observed. However, the FTIR analysis suggested the substitution of carbonate in the apatite structures, compromising the purity of HAp. Thermal degradation studies were not reported.

Other methods that have been explored to produce HAp/CS microparticles are: water-in-oil (W/O) emulsion [41]; supercritical assisted atomization [42], spray-coagulation [43], electro-spray coagulation [44], and dispersion polymerization [45].

In this work, n-HAp/CS microparticles mimicking bone composition, and containing highly pure HAp nanoparticles, were produced in a two-stage process. First, homogeneous and stable n-HAp/CS dispersions were produced using an innovative fast stirring set-up. With the aim of analysing the effect of pH on the final products, the dispersions were produced at two different pH values, right above and below the chitosan pKa. For the case of pH below chitosan pKa, special care was taken to assure pH values higher than 5.0 to avoid solubilisation of HAp. In a second step, hybrid microparticles were produced from the n-HAp/CS dispersions by spray drying. The effect of KCl content was also studied, since this salt is present in the original HAp paste used.

The n-HAp/CS nanodispersions were characterized by measuring particle size and zeta potential by static and electrophoretic light scattering methods, respectively. The produced microparticles were characterized by scanning electron microscopy (SEM) coupled with energy-dispersive X-ray spectroscopy (EDS), thermogravimetry (TG/DTG) and differential scanning calorimetry (DSC). In order to infer the effect of spray-drying conditions on material degradation, freeze-dried samples were also produced and characterized.

2. Materials and methods

2.1. Materials

The n-HAp/CS dispersions were prepared by using the chitosan brand 90/200/A1 from Biolog-Biotechnologie GmbH (Germany), composed of flakes with size <200 μm, with a deacetylation degree of 91.9%, and dynamic viscosity of 128 mPa·s (1% at 20 °C in 1% acetic acid solution). The hydroxyapatite aqueous paste used, nanoXIM-CarePaste, was supplied by Fluidinova S.A. It is composed of 15.5 ± 0.5 wt.% of HAp nanoparticles with particle size <50 nm, 4.5 ± 0.5 wt.% KCl and a water content ≤ 81.0 wt.%. Acetic acid, sodium hydroxide and sodium acetate tri-hydrate of analytical grade from Sigma Aldrich were used to prepare the solutions.

2.2. Dispersions preparation

Aqueous nanodispersions of HAp in the presence of chitosan, with a HAp concentration of 20 g/l, were prepared by using a high speed dispersing and homogenizing device Miccra D-9 at speed rate of 11,000 rpm. The mixing system was designed such that the HAp paste was injected into the chitosan solution inside the vessel right below the dispersing tip, as shown in Fig. 1. The mixing time using a pump rate of 240 rpm (32 ml/min) was estimated to be less than 100 ms. All n-HAp/CS nanodispersions were prepared with HAp to chitosan weight ratio of 70/30, since this ratio represents the typical bone composition.

Two different pH values were considered, one lower and one higher than the chitosan pKa (5.5 and 7.0, respectively). For the preparation of the nanodispersion with lower pH, labelled as ‘‘HApCS-5.5”, a pre-mixed solution prepared by adding a chitosan solution (3.0%, w/v) with an acetate buffer of pH = 5.5 was added to the reactor vessel, followed by the injection of the HAp paste (15%, w/w) continuously at a pump rate of 240 rpm into the chitosan solution. The sample with higher pH, labelled ‘‘HApCS-7.0”, was prepared following the same procedure but with an extra final step consisting in the dropwise addition of NaOH 1 M under fast stirring until neutralization.

The nanoXIM-CarePaste used in this work contains ~4.5 wt.% KCl. In order to study the effect of KCl presence on the stability of the produced nanodispersions and morphology of the final

microparticles, samples were obtained both with the original, unwashed paste and with a paste washed 3 times with distilled water to remove the salt. The potassium content of the washed paste was found to be 15.0 ± 0.9 ppm, determined by Atomic Absorption Spectroscopy (AAS).

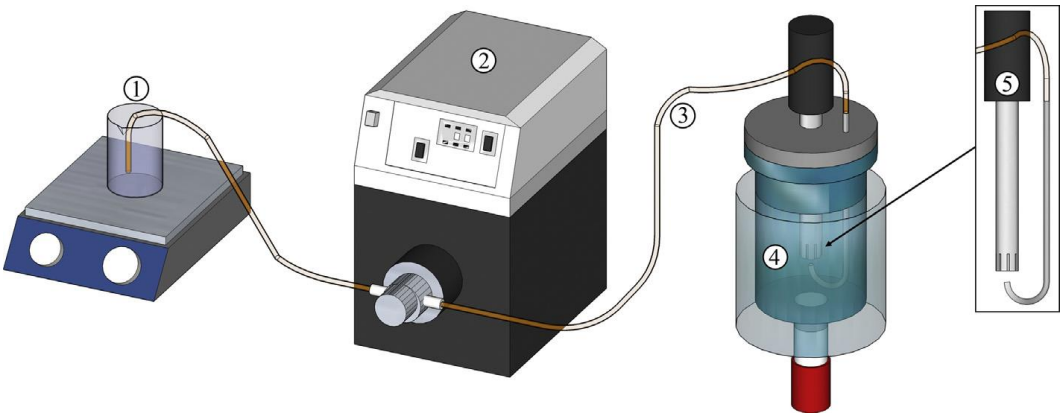

Fig. 1. Experimental setup used to prepare the n-HAp/CS nanodispersions: (1) Beaker containing the n-HAp, nanoXIM-CarePaste, under stirring; (2) peristaltic pump; (3) tubing; (4) vessel containing the CS solution and buffer; (5) ultraturrax.

2.3. Microparticles preparation

The n-HAp/CS hybrid microparticles were prepared by spraydrying a volume of 150 ml of the prepared dispersions. The used apparatus was a Mini Spray Dryer B-290 from Büchi equipped with a nozzle of 0.7 mm of diameter and the operating conditions were: inlet temperature of 170 °C; aspiration at 100%; spray gas flow at 30% (approximately 6 L/min); and pump rate at 15% (approximately 4.5 ml/min). The spray-drying yield was estimated as the ratio between the weight of the recovered powder and the initially used weight of solids of the atomized nanodispersions.

2.4. Preparation of freeze-dried samples

In order to infer the effect of spray-drying conditions on the micro particles' thermal degradation, samples prepared by direct freeze-drying of the obtained dispersions were produced. For that, 10 ml of each sample were firstly congealed by storing in a freezer for about 24 h followed by freeze-drying in a VirTis BenchTop 6 K Freeze Dryer (model nº 6KBTEL) during 48 h.

2.5. Characterization of dispersions

Particle size of the obtained dispersions, HApCS-5.5 and HApCS-7.0, was determined by using a Mastersizer 3000 laser diffraction analyser from Malvern Instruments. The effect of pH on dispersions stability was studied by using the Zetasizer Nano ZS from Malvern Instrument coupled with a MPT-2 Autotitrator using NaOH (0.25 M) as the titrant solution.

2.6. Characterization of microparticles

Morphology of the spray-dried microparticles was inspected by scanning electron microscopy (SEM) coupled with Energydispersive X-ray spectroscopy (EDS) by using a Phenom Pro microscope from Phenom World. High resolution images were obtained by High resolution (Schottky) Environmental Scanning Electron Microscope with X-ray Microanalysis and Backscattered Electron Diffraction Pattern Analysis (FEG-ESEM/EDS/EBSD) using a FEI Quanta 400 FEG ESEM / EDAX Genesis X4M.

FT-IR spectra were recorded in a FT-IR BOMEN (model MB 104) in transmittance mode by using the KBr pellet technique at a concentration of about 1% (w/w). Scanning was carried out between 500 and 4000 cm^{-1} at a resolution of 4 cm^{-1} and co-adding sixty-four scans. The

characterization of the HApCS-5.5 and HApCS-7.0 microparticles was achieved by analogy with the spectra of HAp and chitosan standard samples. Thermal characterization was obtained by thermogravimetry (TG) using a TG 209 F3 Tarsus® and differential scanning calorimetry (DSC) using a DSC 200 F3 Maia. The reproducibility of the experimental procedure was checked based on 3 replicas.

3. Results and discussion

3.1. Preparation and characterization of the hybrid dispersions

Table 1 shows the number mean particle size and zeta potential values obtained for the HAp dispersions produced at pH of 5.5, alone and in the presence of chitosan, both with and without KCl. Monodispersed distributions were obtained in all cases, with larger particle sizes for the hybrid ones when compared with the HAp alone, but with no significant differences derived from the presence of KCl. In terms of charge stability, the HAp dispersions containing KCl presented higher zeta potential values (>30 mV), which indicate that the salt improves the stability of the HAp dispersion. In the case of HApCS-5.5 dispersions with KCl a good zeta potential value (>30 mV) was obtained, but an even higher zeta potential value was obtained for the HApCS-5.5 sample without KCl, which shows that chitosan also acts as an effective stabilizer besides providing the aforementioned list of desirable properties for bone repair and regeneration.

Table 1. Zeta potential (ZP) and number mean particle size values obtained for nanodispersions of HAp with and without KCl.

Sample	ZP (mv)	Number mean (nm)
HAp/water without KCl	24.1 ± 0.6	43.0 ± 3.1
HAp/water with KCl	31.2 ± 0.3	42.7 ± 4.8
HAp/CS-5.5 without KCl	33.7 ± 0.2	198 ± 25
HAp/CS-5.5 with KCl	32.8 ± 0.2	222 ± 20

Particle sizes obtained by laser diffraction for samples HApCS-5.5 and HApCS-7.0 are summarized in Table 2, reported as particle size percentiles in volume (Dv10, Dv50 and Dv90), where, for example, Dv50 means the maximum particle diameter below which 50% of the sample volume exists. n-HAp/CS nanodispersions prepared at pH ~ 5.5 presented a Dv50 of 28.4 μm, while the ones produced at higher pH (~7.0) presented a Dv50 of 72.2 lm suggesting not only that HAp nanoparticles remain as clusters when dispersed in chitosan solutions, but also that the higher-pH condition produces larger clusters. Relative to zeta potential measurements, nanodispersions of HAp in water with an initial pH of approximately 9.0 and a zeta potential around 29 mV, showed a tendency to decrease as the pH decreases (see Fig. 2). However, with the use of chitosan, a high zeta potential was obtained even at low pH values and, in contrast to what happens with HAp alone, a linear tendency of zeta potential to decrease with the increase of pH is observed (Fig. 2).

Table 2. Particle size percentiles in volume obtained for HApCS-5.5 and HApCS-7.0 samples from laser diffraction measurements.

Sample	Dv10 (μm)	Dv50 (μm)	Dv90 (μm)
HApCS-5.5	14.8	28.4	50.2
HApCS-7.0	23.5	72.2	165

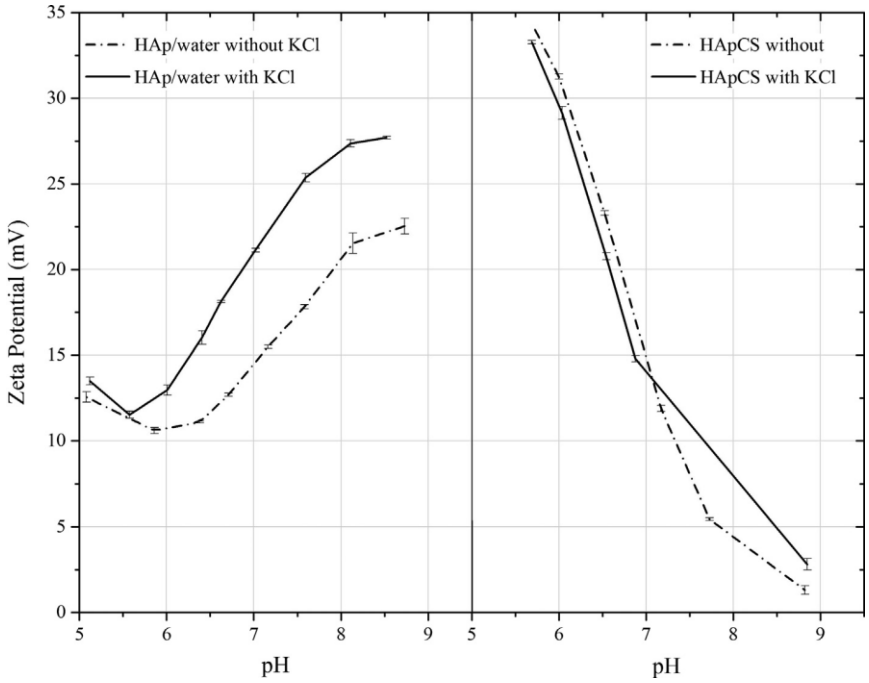

Fig. 2. Zeta potential tendency with changing pH for: HAp dispersion (CH_3COOH 0.25 M as titrant); and n-HAp/CS nanodispersion (NaOH 0.25 and 1 M solutions as titrants).

3.2. Characterization of the n-Hap/CS hybrid microparticles

n-HAp/CS hybrid microparticles were successfully produced by spray drying with average yields of 62 and 52% for the HApCS-5.5 and HApCS-7.0 samples, respectively.

Fig. 3 shows SEM images of microparticles obtained with the unwashed, i.e. with KCl, HAp paste. The formation of mushroom and doughnut-like microparticles was observed for the HApCS-5.5 sample. This type of morphology is ruled by hydrodynamics, both in- and outside the droplet, causing a droplet-transformation phenomenon going from a spherical to mushroom-like, to a final doughnut shape, as described by some authors [32,46].When compared to analogous spherical microparticles, studies have found that particles with torus geometry (doughnut) present advantages such as a higher stability for long-term storage in an aqueous environment and after undergoing processes such as freeze-drying [47].

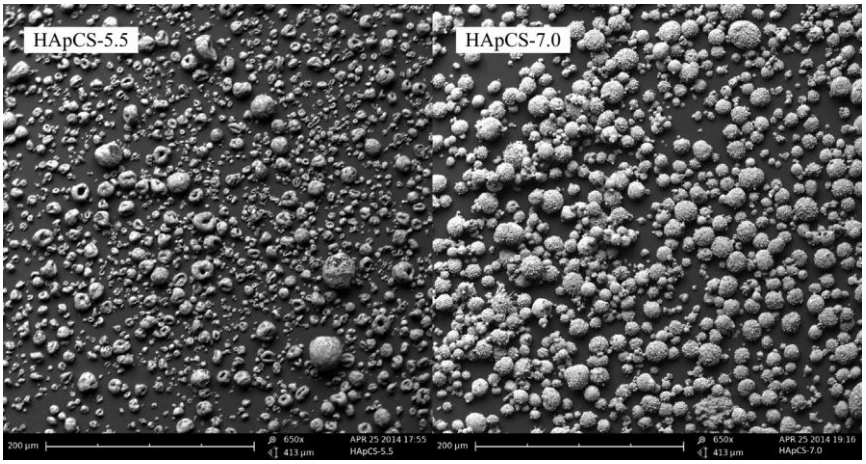

Fig. 3. High resolution SEM images of HAp/CS microparticles obtained with unwashed, with KCl, HAp paste.

The HApCS-7.0 derived powder, on the other hand, presents better-defined spherical shape with spikes on the surface (see Fig. 4). The maximum structural stability of spheres is the main reason why this shape is typically produced by spray drying. Drying temperature and velocity of the carrier gas are the main parameters influencing hydrodynamics of the droplets, but variables such as viscosity, density and concentration of the dispersions, as well as size of the nanoparticles are also fundamental factors influencing the final morphology of the microparticles [32,46].

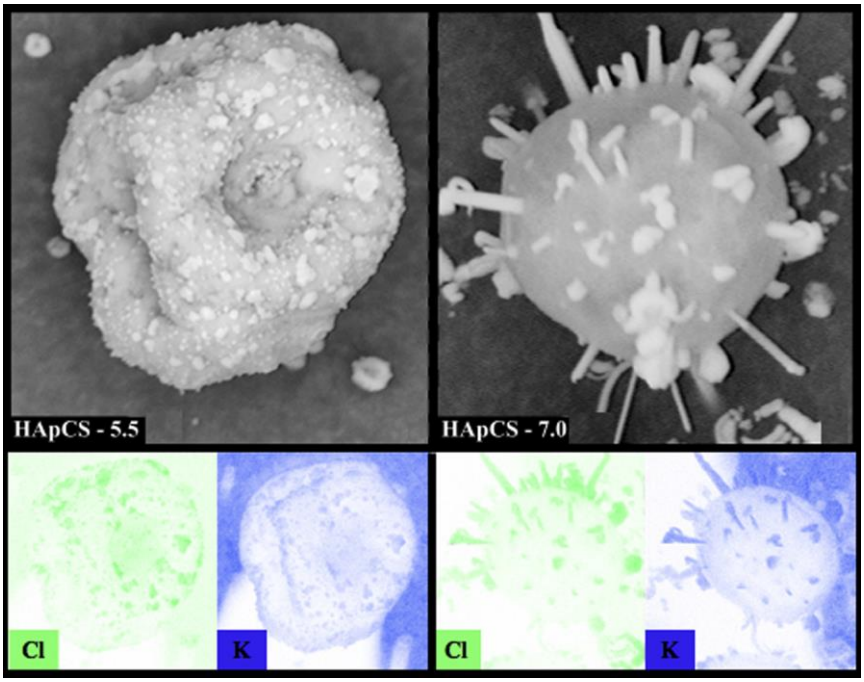

Fig. 4. Elemental mapping by EDS of HAp/CS microparticles obtained with unwashed, with KCl, HAp paste, Cl in green and K in blue.

Elemental mapping by EDS (Fig. 4) allowed the identification of the spikes observed in the HApCS-7.0 microparticles as KCl microcrystals. The salt was also detected in the HApCS-5.5 microparticles, even the crystals were significantly smaller and presented quite distinct morphology. As it is desired to produce microparticles with high purity, containing mainly HAp and chitosan, KCl appears as a contaminant in large quantities as seen in the SEM images. In addition, it was proven that it has no beneficial effect on the stability of the n-HAp/CS dispersions and it could eventually create a hypertonic environment that could cause an inhibitory effect on cell metabolism [48].

High-resolution images from the microparticles produced from the nanodispersions prepared with washed HAp paste are shown in Fig. 5. HApCS-7.0 microparticles seem to have a tendency to form strong agglomerates; this phenomenon is not observed in the case of the HApCS-5.5 microparticles. No traces of KCl salts were detected by EDS, and HAp rod-like particles of nanometer sizes can be observed at the surface of the microparticles, for both samples. HApCS-5.5 microparticles present a rough surface that can be beneficial for biomedical applications, since it has been proven non-smooth surfaces can enhance cell adhesion and proliferation [49]. Particle sizes of the microparticles were obtained by image analysis; very similar number mean values, corresponding to 6.83 μm and 6.67 μm for HApCS-5.5 and HApCS-7.0 respectively, were obtained for both samples. In terms of average size in volume, HApCS-7.0 sample presented a slightly smaller value of 12.8 μm based on the circle equivalent diameter of 1493 particles, compared to an average size in volume of 15.8 μm for the HApCS-5.5 sample based on the circle equivalent diameter of 1072 particles. These results suggest that HApCS-5.5 presented a few

particles with larger sizes when compared to HApCS-7.0 sample, but also large amount of particles with small sizes. It is important to point out as well that HApCS-7.0 microparticles formed agglomerates of up to approximately 170 μm.

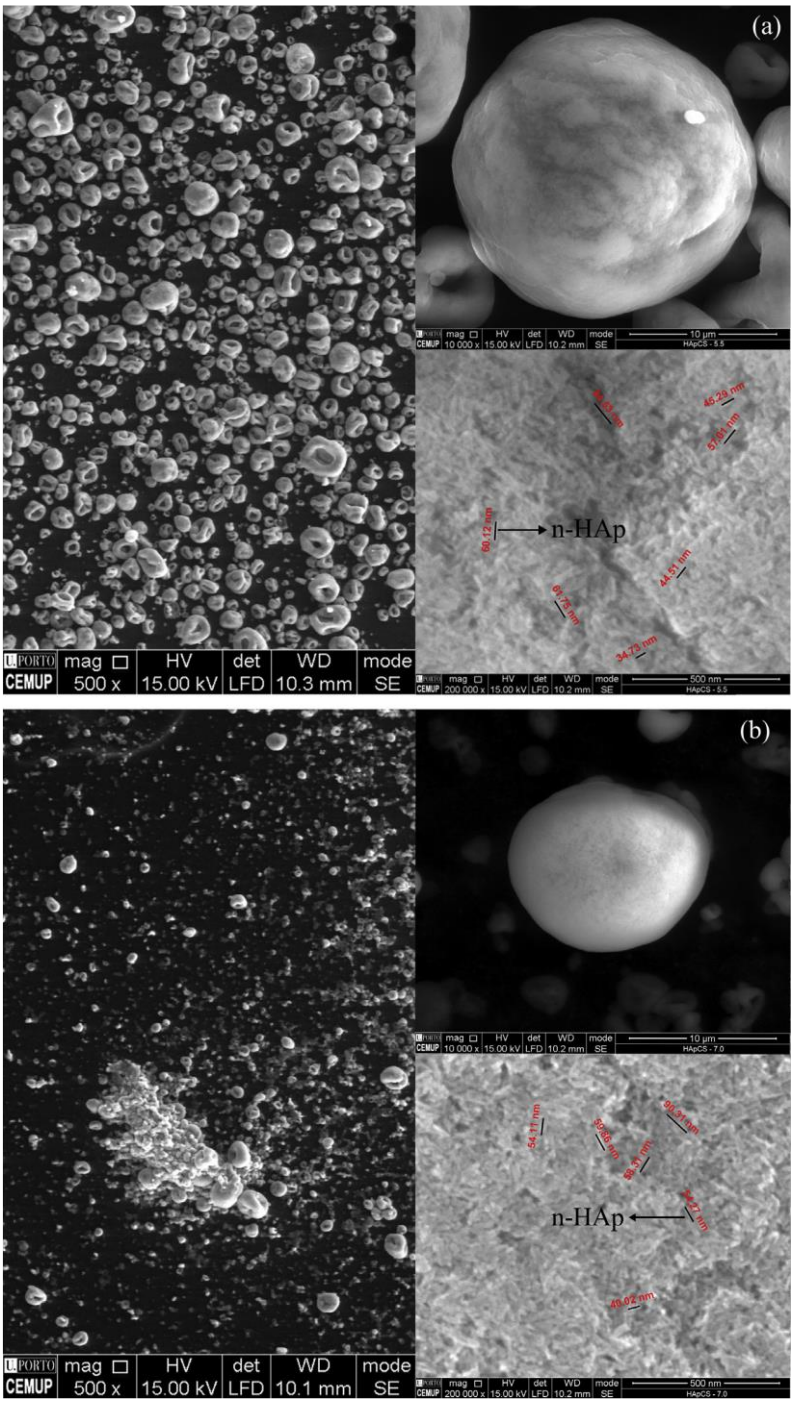

Fig. 5. High resolution SEM images of HAp/CS microparticles obtained with washed, without KCl, HAp paste: (a) HApCS-5.5 and (b) HApCS-7.0. Images on the left were obtained at a magnification of 500x; images on the right were obtained at 10,000x (top, zoom of a single particle), and 200,000x (bottom, zoom of a particle's surface).

The IR spectra of HApCS-5.5 and HApCS-7.0, and the spray-dried HAp paste and chitosan, used as standard samples, are shown in Fig. 6. Spray-dried HAp-paste spectra presented the typical bands of phosphate group, PO_4. Peaks at 1093 and 1032 cm^{-1} correspond to a triply degenerated

asymmetric stretching mode vibration of the P–O bond of the phosphate group. A non-degenerated symmetric stretching mode of the P–O bond of the phosphate group is observed at 962 cm^{-1}. Peaks at 603 and 566 cm^{-1} correspond to a triply degenerated bending mode of the O–P–O bond. Peak at 632 cm^{-1} is assigned to the hydroxyl group deformation mode and it is considered to be overlapped with asymmetric P–O stretching vibration of PO_4^{3-}. Band at 3567 cm^{-1} was attributed to the stretching mode of the hydroxyl group, OH, while bands at 3421 and 1653 cm^{-1} are assigned to absorbed water, which appeared even when precautions were taken to eliminate moisture from the samples before analysis.

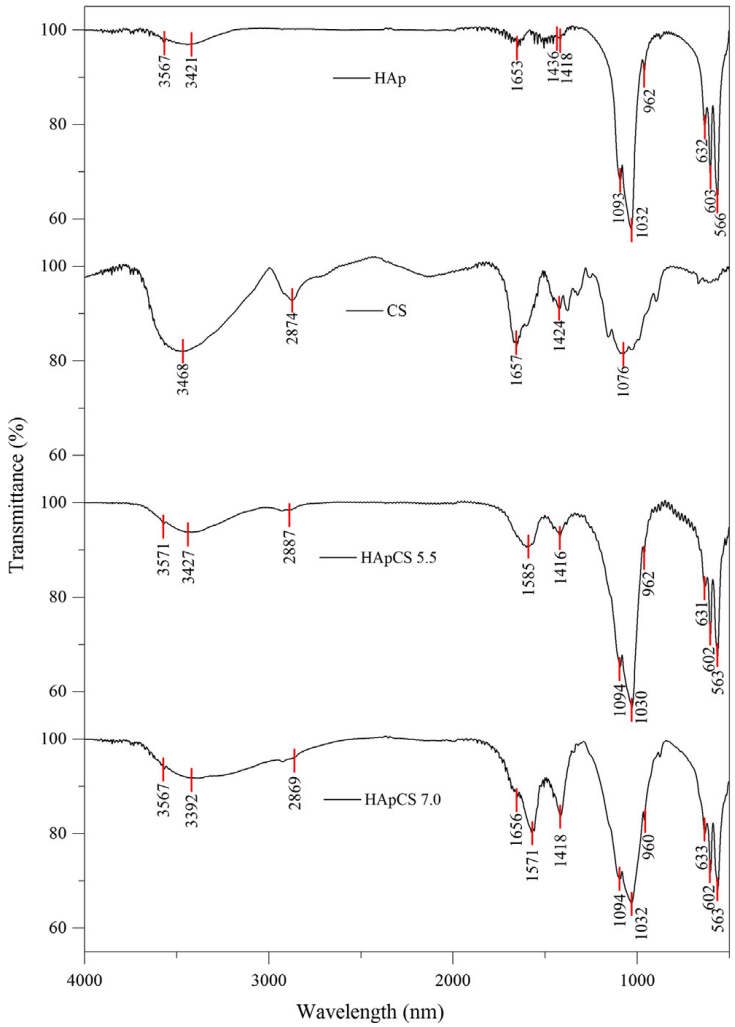

Fig. 6. Infrared spectra of standards HAp and chitosan, HApCS-5.5 and HApCS-7.0.

The characteristic groups of chitosan were also confirmed in the corresponding chitosan spectrum. The band at 3468 cm^{-1} was assigned to stretching mode of the OH group, overlapped with stretching mode of NH. Peaks at 1300–1450 cm^{-1} may correspond to a combination of CN–NH, CH_2–OH and CH_3 bands [50]. Bands at 2874 and 1424 cm^{-1} can be attributed to CH stretching and bending vibrations respectively, while peaks at 1657 and 1076 cm^{-1} correspond to NH, and C–O–C groups correspondingly.

IR spectra of both hybrid microparticles, HApCS-5.5 and HApCS-7.0, presented all typical bands of the characteristic groups of Hap and chitosan, proving that the HAp nanoparticles were successfully incorporated into the chitosan matrix. For primary amines, the N–H bending (scissoring) vibration is observed in the region 1650–1580 cm^{-1} of the spectrum. This band of

medium – strong intensity appears at slightly higher frequencies when the primary amine is associated with other groups. In particular, when the amine is protonated, the NH^{3+} group can form ionic bonds with opposite charged groups. In this case the NH^{3+} group of the primary amine will give rise to absorptions in the regions 1600-1575 and 1550–1504 cm^{-1}, close to the corresponding bands of the CH_3 group [51].

Both samples presented bands in the absorption region of the primary amine group, however, some differences are observed. HApCS-5.5 spectrum shows only one peak at 1585 cm^{-1}, while HApCS-7.0 spectrum shows two peaks in this region (1656 and 1571 cm^{-1}). The peak at 1656 cm^{-1} can be attributed to the N–H of the NH_2 group due to the neutralization of the amine groups when increasing the pH of the nanodispersions. The peaks observed near 1580 cm^{-1}, in both HApCS-5.5 and HApCS-7.0, can be attributed to a possible formation of ionic bonds between NH^{3+} from chitosan and PO_4^{3-} from hydroxyapatite. These differences show that the pH at which the nanodispersions were prepared affected the chemical interactions between HAp and chitosan, leading to final products with different properties.

Results obtained from TG/DTG analysis of all the prepared samples are shown in Fig. 7. For comparative purposes, solutions of chitosan in acetic acid were prepared and the pH was adjusted above and below 6.5, labelled CS-5.5 and CS-7.0, followed by spray-drying to obtain microparticles of such solutions. The first mass loss is observed between 30 and 100 °C for all cases and it is attributed to water evaporation. Another peak is observed between 100 and 170 °C in the curves of both CS-5.5 and HApCS-5.5, which can be related to the degradation of the acid used in the preparation of such samples. This peak is absent in the thermograms of the samples prepared at higher pH since the acid was neutralized by the addition of base to increase the pH. The peak observed around 730 °C in the HApCS-7.0 thermograms can be related to the degradation of the base used to increase the pH of this dispersion.

Finally, a mass loss observed between 200-310 °C can be attributed to the thermal degradation of chitosan. This degradation step appears approximately at the same temperature (240 °C) for all samples analyzed. Moreover, the HApCS-5.5 curves present what seems to be a retardation of the decomposition of the polymer at 400 °C. It is noteworthy to point out that the hybrid samples show different patterns of degradation for chitosan that could be associated with differences in the interactions between chitosan and HAp depending on the pH at which the dispersions were prepared.

Both hybrids, HApCS-5.5 and HApCS-7.0, presented similar composition to that one of natural bone (see Table 3). Residual masses near 70% were attributed to HAp since the acid and base used in sample preparation were degraded below 800 °C and HAp degradation was absent. The residual mass obtained agrees with the used HAp content.

The TG-DTG plots obtained for freeze-dried samples, HApCS-5.5-FD and HApCS-7.0-FD, are also shown in Fig. 7. No significant differences are observed when compared to the analogous thermograms of the spray-dried samples HApCS-5.5 and HApCS-7.0 respectively, which proves that the chitosan was not degraded during the spray-drying process at the used conditions.

The DSC plots (Fig. 8) confirm the results obtained by TG-DTG in terms of thermal degradation of chitosan, which has an exothermic peaks near 300 °C. For both, TG and DSC analysis, a good reproducibility was observed since all transitions obtained coincide between batches of the same type of sample, either HApCS-5.5 or HApCS-7.0.

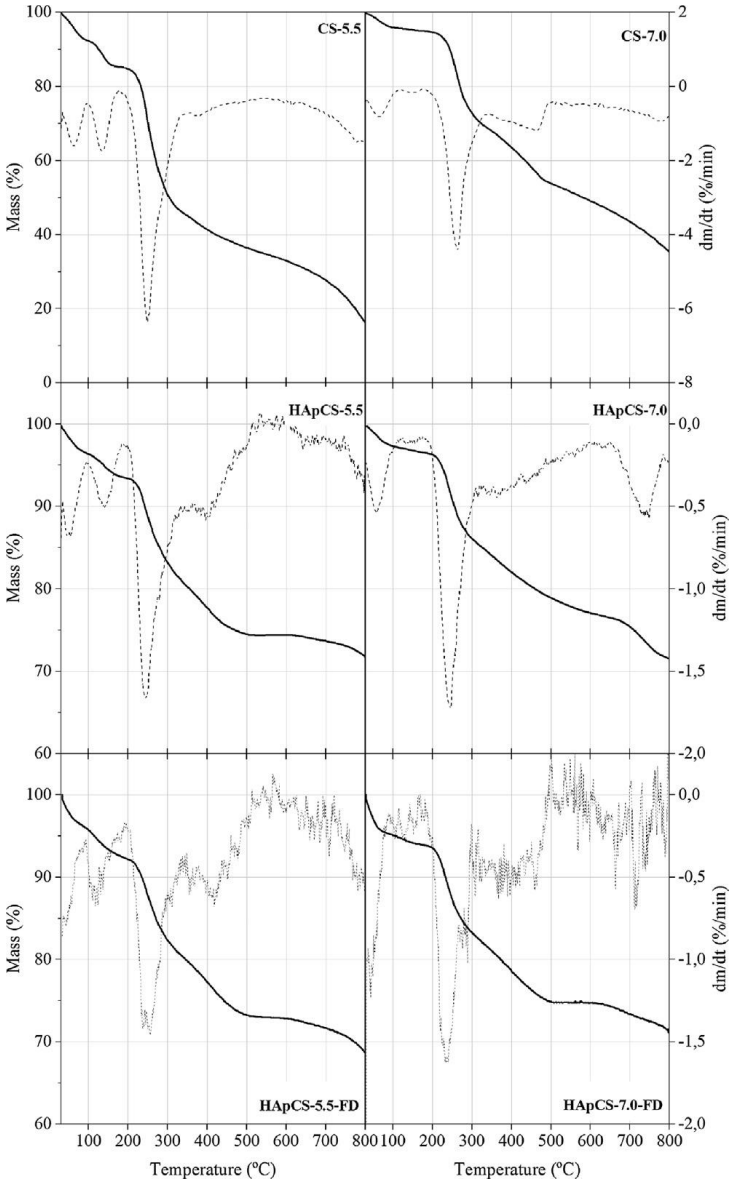

Fig. 7. TG (solid line) and DTG (dash line) of spray-dried HApCS-5.5, HApCS-7.0, CS-5.5, CS-7.0 and freeze-dried samples HApCS-5.5-FD and HApCS-7.0-FD (from 30 to 800 °C at 10 °C/min; N_2 atmosphere).

Table 3. Comparative table of the composition of natural bone relative to the composition of HApCS-5.5 and HApCS-7.0 based on thermal degradation (TG/DTG analysis).

Component	Natural bone	HApCS-5.5	HApCS-7.0
Inorganic	60–70% n-HAp	~72% n-HAp	~71.5% n-HAp
Organic	25–30% collagen	~22% chitosan	~21% chitosan
Water	~5–10%	~6% water and acetic acid	~7.5% water and base

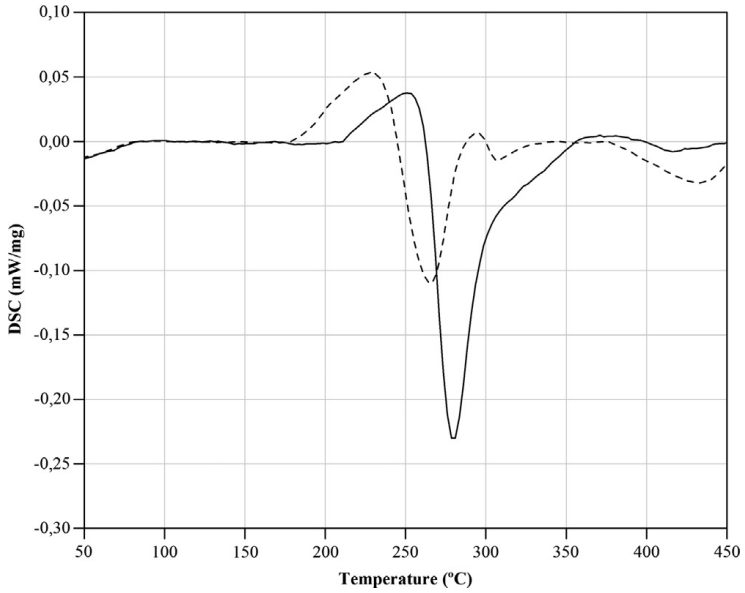

Fig. 8. DSC of HApCS-5.5 (solid line) and HApCS-7.0 (dash line); from 50 to 450 °C at 10 °C/min; N_2 atmosphere.

4. Conclusion

In this study, it was observed that different types of spray-dried microparticles are produced depending on the pH at which the initial nanodispersions were prepared. Dispersions with smaller particle sizes and higher zeta potential values are produced with the n-HAp/CS dispersions with pH < 6.5, compared to dispersions with pH > 6.5. The presence of KCl, a component of the original HAp paste used, has no beneficial effect on the stability of the n-HAp/CS dispersions, and its removal can be easily achieved by a prewashing procedure.

Differences on the spray-dried microparticles due to the effect of pH conditions were also evident from a morphological point of view. Doughnut-like HApCS-5.5 microparticles, with 15.8 lm average size in volume and n-HAp particles homogenously distributed, are preferred over HApCS-7.0 microparticles, which require an extra step in the productive process and also presented a tendency to form large agglomerates.

FTIR analysis of both HApCS-5.5 and HApCS-7.0 showed all typical bands of the characteristic groups of HAp and chitosan, proving that the HAp nanoparticles were successfully incorporated into the chitosan matrix. Evidence of formation of ionic bonds of the primary amine groups, NH^{3+}, was observed which is compatible with ionic bonds formation between NH^{3+} from chitosan and PO_4^{3-} from hydroxyapatite.

The spray-dried microparticles presented different thermal degradation behaviour that can be related to differences in HApchitosan interactions depending on the pH at which the products were prepared. The residual mass from TG results was near 70%, attributed to hydroxyapatite in accordance with the weight ratio pretended. No significant differences were observed between spray-dried and freeze-dried samples, which evidences that chitosan was not degraded during the spray-drying process at the used conditions. The reproducibility of the experimental procedure was checked based on 3 replicas.

Most importantly, hybrid n-HAp/CS microparticles containing 50 nm HAp nanoparticles were produced successfully by spray drying. Besides their beneficial characteristics to design injectable systems or mouldable solid substrates, these microparticles can offer advantages for biomedical

applications, such as bone repair and drug delivery systems. For example, these microcarriers can be loaded with therapeutic and bioactive factors, and incorporated into 3D systems (scaffolds) to enhance functional properties.

Acknowledgements

Financial support for this work was provided by FCT – Portugal and FEDER – Portugal under Programe PT2020 (Project UID/EQ/50020/2013), QREN, ON2, FCT and FEDER (Projects NORTE-07-0162-FEDER-000050, NORTE-07-0124-FEDER-000013 and NORTE-07-0124-FEDER-000014). G. Ruphuy thanks Universidad de Costa Rica (UCR) – Costa Rica and Ministerio de Ciencia Tecnología y Telecomunicaciones (MICITT) – Costa Rica for her scholarship. Authors thank Fluidinova S.A. for providing the nanoXIMCarePaste, and the Centro de Materiais da Universidade do Porto (CEMUP) for the services provided with ESEM analysis.

References

[1] S.M. Amit, S. Xinfeng, G.M. Antonios, Nanocomposite scaffolds for tissue engineering, in: J.D. Bronzino (Ed.), Tissue Engineering and Artificial Organs, CRC Press, 2006. 40-41-40-11.

[2] S.K.L. Levengood, M. Zhang, Chitosan-based scaffolds for bone tissue engineering, J. Mater. Chem. B 2 (2014) 3161.

[3] J. Venkatesan, S.K. Kim, Chitosan composites for bone tissue engineering–an overview, Mar. Drugs 8 (2010) 2252–2266.

[4] S.-Y. Shin, H.-N. Park, K.-H. Kim, M.-H. Lee, Y.S. Choi, Y.-J. Park, Y.-M. Lee, Y. Ku, I.-C. Rhyu, S.-B. Han, Biological evaluation of chitosan nanofiber membrane for guided bone regeneration, J. Periodontol. 76 (2005) 1778–1784.

[5] A.J. Bavariya, P. Andrew Norowski, K. Mark Anderson, P.C. Adatrow, F. Garcia-Godoy, S.H. Stein, J.D. Bumgardner, Evaluation of biocompatibility and degradation of chitosan nanofiber membrane crosslinked with genipin, J. Biomed. Mater. Res. B Appl. Biomater. 102 (2014) 1084–1092.

[6] C.-M. Lehr, J.A. Bouwstra, E.H. Schacht, H.E. Junginger, In vitro evaluation of mucoadhesive properties of chitosan and some other natural polymers, Int. J. Pharm. 78 (1992) 43–48.

[7] P. He, S.S. Davis, L. Illum, In vitro evaluation of the mucoadhesive properties of chitosan microspheres, Int. J. Pharm. 166 (1998) 75–88.

[8] Y.-J. Seol, J.-Y. Lee, Y.-J. Park, Y.-M. Lee, I.-C. Rhyu, S.-J. Lee, S.-B. Han, C.-P. Chung, Chitosan sponges as tissue engineering scaffolds for bone formation, Biotechnol. Lett. 26 (2004) 1037–1041.

[9] H. Ueno, H. Yamada, I. Tanaka, N. Kaba, M. Matsuura, M. Okumura, T. Kadosawa, T. Fujinaga, Accelerating effects of chitosan for healing at early phase of experimental open wound in dogs, Biomaterials 20 (1999) 1407–1414.

[10] A.K. Azad, N. Sermsintham, S. Chandrkrachang, W.F. Stevens, Chitosan membrane as a wound-healing dressing: Characterization and clinical application, J. Biomed. Mater. Res. B Appl. Biomater. 69B (2004) 216–222.

[11] A. Di Martino, M. Sittinger, M.V. Risbud, Chitosan: A versatile biopolymer for orthopaedic tissue-engineering, Biomaterials 26 (2005) 5983–5990.

[12] F. Croisier, C. Jérôme, Chitosan-based biomaterials for tissue engineering, Eur. Polymer J. 49 (2013) 780–792.

[13] C. Ji, N. Annabi, A. Khademhosseini, F. Dehghani, Fabrication of porous chitosan scaffolds for soft tissue engineering using dense gas CO2, Acta Biomater. 7 (2011) 1653–1664.

[14] N. Siddiqui, K. Pramanik, E. Jabbari, Osteogenic differentiation of human mesenchymal stem cells in freeze-gelled chitosan/nano b-tricalcium phosphate porous scaffolds crosslinked with genipin, Mater. Sci. Eng., C 54 (2015) 76–83.

[15] J.V. Araujo, N. Davidenko, M. Danner, R.E. Cameron, S.M. Best, Novel porous scaffolds of pH responsive chitosan/carrageenan-based polyelectrolyte complexes for tissue engineering, J. Biomed. Mater. Res., Part A 102 (2014) 4415–4426.

[16] M.Z. Albanna, T.H. Bou-Akl, O. Blowytsky, H.L. Walters Iii, H.W.T. Matthew, Chitosan fibers with improved biological and mechanical properties for tissue engineering applications, J. Mech. Behav. Biomed. Mater. 20 (2013) 217–226.

[17] Y.F. Aklog, A.K. Dutta, H. Izawa, M. Morimoto, H. Saimoto, S. Ifuku, Preparation of chitosan nanofibers from completely deacetylated chitosan powder by a downsizing process, Int. J. Biol. Macromol. 72 (2015) 1191–1195.

[18] C.A. Custódio, M.T. Cerqueira, A.P. Marques, R.L. Reis, J.F. Mano, Cell selective chitosan microparticles as injectable cell carriers for tissue regeneration, Biomaterials 43 (2015) 23–31.

[19] R. Obaidat, B. Tashtoush, M. Bayan, R.T. Al Bustami, M. Alnaief, Drying using supercritical fluid technology as a potential method for preparation of chitosan aerogel microparticles, AAPS PharmSciTech (2015) 1–10.

[20] Y.-B. Shen, Z. Du, Q. Wang, Y.-X. Guan, S.-J. Yao, Preparation of chitosan microparticles with diverse molecular weights using supercritical fluid assisted atomization introduced by hydrodynamic cavitation mixer, Powder Technol. 254 (2014) 416–424.

[21] A.R. Costa-Pinto, R.L. Reis, N.M. Neves, Scaffolds based bone tissue engineering: the role of chitosan, Tissue Eng.. Part B, Rev. 17 (2011) 331–347.

[22] O.C. Wilson, J.R. Hull, Surface modification of nanophase hydroxyapatite with chitosan, Mater. Sci. Eng., C 28 (2008) 434–437.

[23] M. Supova, Problem of hydroxyapatite dispersion in polymer matrices: a review, J Mater Sci Mater Med 20 (2009) 1201–1213.

[24] T.J. Webster, C. Ergun, R.H. Doremus, R.W. Siegel, R. Bizios, Enhanced functions of osteoblasts on nanophase ceramics, Biomaterials 21 (2000) 1803–1810.

[25] L. Kong, Y. Gao, W. Cao, Y. Gong, N. Zhao, X. Zhang, Preparation and characterization of nano-hydroxyapatite/chitosan composite scaffolds, J. Biomed. Mater. Res., Part A 75A (2005) 275–282.

[26] J.M. Oliveira, M.T. Rodrigues, S.S. Silva, P.B. Malafaya, M.E. Gomes, C.A. Viegas, I.R. Dias, J.T. Azevedo, J.F. Mano, R.L. Reis, Novel hydroxyapatite/chitosan bilayered scaffold for osteochondral tissue-engineering applications: Scaffold design and its performance when seeded with goat bone marrow stromal cells, Biomaterials 27 (2006) 6123–6137.

[27] W.W. Thein-Han, R.D.K. Misra, Biomimetic chitosan–nanohydroxyapatite composite scaffolds for bone tissue engineering, Acta Biomater. 5 (2009) 1182–1197.

[28] G. Silva, P. Ducheyne, R. Reis, Materials in particulate form for tissue engineering. 1. Basic concepts, J. Tissue Eng. Regenerative Med. 1 (2007) 4–24.

[29] G. Silva, O. Coutinho, P. Ducheyne, R. Reis, Materials in particulate form for tissue engineering. 2. Applications in bone, J. Tissue Eng. Regenerative Med. 1 (2007) 97–109.

[30] M.B. Oliveira, J.F. Mano, Polymer-based microparticles in tissue engineering and regenerative medicine, Biotechnol. Prog. 27 (2011) 897–912.

[31] K. Okuyama, M. Abdullah, I. Wuled Lenggoro, F. Iskandar, Preparation of functional nanostructured particles by spray drying, Adv. Powder Technol. 17 (2006) 587–611.

[32] A.B.D. Nandiyanto, K. Okuyama, Progress in developing spray-drying methods for the production of controlled morphology particles: From the nanometer to submicrometer size ranges, Adv. Powder Technol. 22 (2011) 1–19.

[33] M.I. Dias, I.C.F.R. Ferreira, M.F. Barreiro, Microencapsulation of bioactives for food applications, Food Funct. 6 (2015) 1035–1052.

[34] A. Ribeiro, G. Ruphuy, J.C. Lopes, M.M. Dias, L. Barros, F. Barreiro, I.C.F.R. Ferreira, Spray-drying microencapsulation of synergistic antioxidant mushroom extracts and their use as functional food ingredients, Food Chem. 188 (2015) 612–618.

[35] K. Sollohub, K. Cal, Spray drying technique: II. Current applications in pharmaceutical technology, J. Pharm. Sci. 99 (2010) 587–597.

[36] Y. Song, S. Tan, J. Sun, J. Zhang, M. Wu, Q. Wu, J. Yang, Synthesis and sustained release property of drug-loaded chitosan microspheres by spray drying technique, Am. J. Macromol. Sci. 2 (2015) 1–10.

[37] A.C. Lima, P. Sher, J.F. Mano, Production methodologies of polymeric and hydrogel particles for drug delivery applications, Expert Opin. Drug Del. 9 (2012) 231–248.

[38] C. Peniche, Y. Solís, N. Davidenko, R. García, Chitosan/hydroxyapatite-based composites, Biotecnología Apl. 27 (2010) 202–210.

[39] O.C. Wilson, J.R. Hull, Surface modification of nanophase hydroxyapatite with chitosan, Mater. Sci. Eng C-Biomim. Supramol. Syst. 28 (2008) 434–437.

[40] T. Bassargan, G. Nasün-Saygılı, Spray dried mesoporous hydroxyapatitechitosan biocomposites, Polym.-Plast. Technol. Eng. (2015).

[41] C.-C. Ding, S.-H. Teng, H. Pan, In-situ generation of chitosan/hydroxyapatite composite microspheres for biomedical application, Mater. Lett. 79 (2012) 72–74.

[42] E. Reverchon, R. Adami, Supercritical assisted atomization to produce nanostructured chitosan-hydroxyapatite microparticles for biomedical application, Powder Technol. 246 (2013) 441–447.

[43] P. Granja, A. Silva, J.P. Borges, C. Barrias, I. Amaral, Preparation and Characterization of Injectable Chitosan-Hydroxyapatite Microspheres, in: Key Engineering Materials, Trans Tech Publ, 2004, pp. 573–576.

[44] J. Chen, P. Pan, Y. Zhang, S. Zhong, Q. Zhang, Preparation of chitosan/nano hydroxyapatite organic–inorganic hybrid microspheres for bone repair, Colloids Surf., B 134 (2015) 401–407.

[45] M. Sivakumar, I. Manjubala, K. Panduranga Rao, Preparation, characterization and in-vitro release of gentamicin from coralline hydroxyapatite–chitosan composite microspheres, Carbohydr. Polym. 49 (2002) 281–288.

[46] F. Iskandar, L. Gradon, K. Okuyama, Control of the morphology of nanostructured particles prepared by the spray drying of a nanoparticle sol, J. Colloid Interface Sci. 265 (2003) 296–303.

[47] S. Ungphaiboon, D. Attia, G.G. d'Ayala, P. Sansongsak, F. Cellesi, N. Tirelli, Materials for microencapsulation: what toroidal particles (''doughnuts") can do better than spherical beads, Soft Matter 6 (2010) 4070–4083.

[48] R.-I. Hata, Age-dependent changes in collagen metabolism and response to hypertonic culture conditions of rat aortic smooth muscle cells and skin fibroblasts, Cell Biol. Int. Rep. 14 (1990) 25–33.

[49] S. Huang, X. Fu, Cell behavior on microparticles with different surface morphology, J. Alloy. Compd. 493 (2010) 246–251.

[50] I.V. Fadeeva, S.M. Barinov, A.Y. Fedotov, V.S. Komlev, Interactions of calcium phosphates with chitosan, Dokl. Chem. 441 (2011) 387–390.

[51] R.M. Silverstein, F.X. Webster, D. Kiemle, D.L. Bryce, Spectrometric Identification of Organic Compounds, John Wiley & Sons, 2014.